Electronic Supplementary Material (ESI) for Nanoscale.

Supporting Information for

Controlled defect creation and removal in graphene and MoS_2 monolayers

D.W. Li,[±,a] Q.M. Zou,[±,a] X. Huang,[a] H. Rabiee Golgir,[a] K. Keramatnejad,[a] J.F. Song,[b,c] Z.Y. Xiao,[b,c] L.S Fan,[a] X. Hong,[b,c] L. Jiang,[d] J.F. Silvain,[e] S. Sun,[b,c,f] and Y.F. Lu*[,a]

[a] Department of Electrical and Computer Engineering, University of Nebraska-Lincoln, Lincoln, NE 68588-0511, United States
[b] Department of Physics and Astronomy, University of Nebraska-Lincoln, Lincoln, NE 68588-0511, United States
[c] Nebraska Center for Materials and Nanoscience, University of Nebraska-Lincoln, NE 68588-0299, United States
[d] School of Mechanical Engineering, Beijing Institute of Technology, Beijing, 100081, China
[e] Institut de Chimie de la Matière Condensée de Bordeaux, Avenue du Docteur Albert Schweitzer F-33608 Pessac Cedex, France
[f] National Laboratory for Infrared Physics, Shanghai Institute of Technical Physics, Chinese Academy of Sciences, Shanghai, 200083, China

* Corresponding author, E-mail: ylu2@unl.edu
± D.W. Li and Q,M, Zou contributed equally to this work.

Contents:

S1. Sputtering Time Dependence of Al_2O_3 Film Thickness

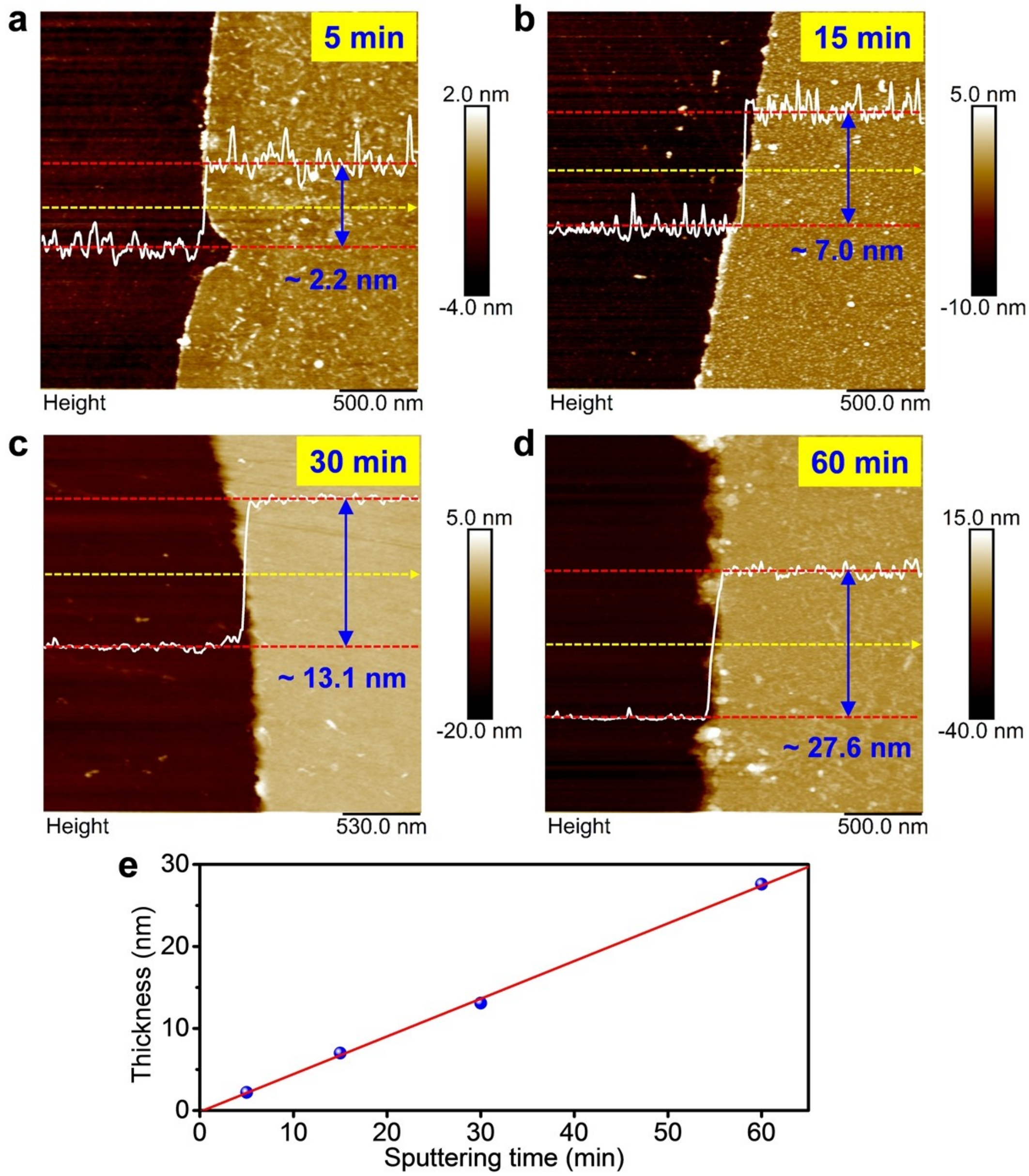

Fig. S1. (a-d) AFM topography images of the Al_2O_3 thin films deposited on SiO_2/Si substrate with a power of 100 W for (a) 5 min, (b) 15 min, (c) 30 min, and (d) 60 min. Insets in (a-d) show the cross-sectional profiles along the yellow dotted lines in the corresponding images. (e) The thickness of Al_2O_3 thin film as a function of sputtering time with a linear fit.

S2. Controlled Creation of Defects in Graphene Bilayers

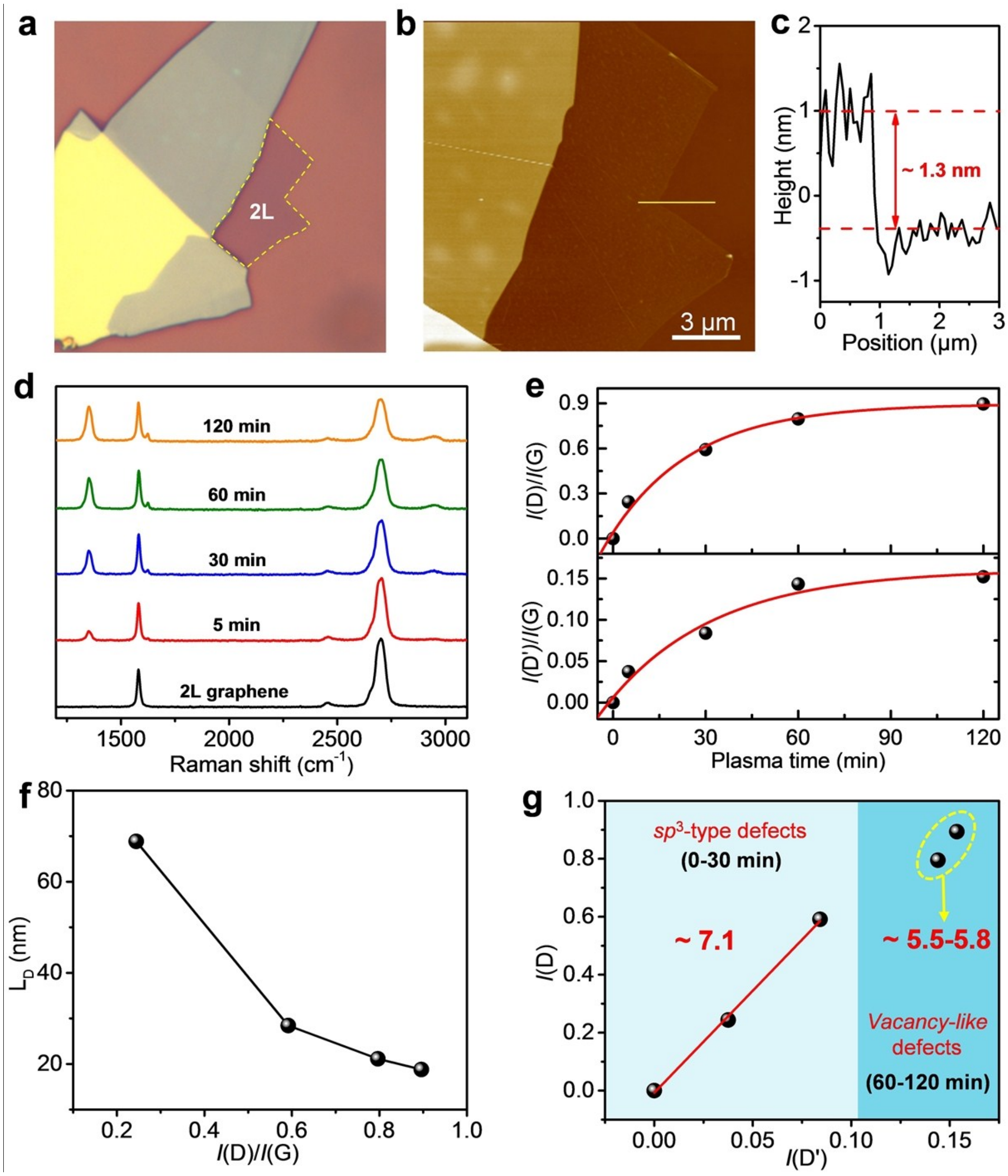

Fig. S2. Controlled creation of defects in graphene bilayers via Al_2O_3 plasma treatment. (a) Optical and (b) AFM images of an exfoilated bilayer graphene transferred onto SiO_2/Si substrate. Scale bar: 3 μm. (c) Cross-sectional profile along the yellow solid line in (b), confirming its bilayer characteristics. (d) Raman spectra of the same bilayer graphene in (a) as a function of Al_2O_3 plasma treatment time. (e) The I_D/I_G (top) and $I_{D'}/I_G$ (bottom) ratio as a function of plasma exposure time. (f) L_D with respect to I_D/I_G ratio. (g) I_D versus $I_{D'}$ in bilayer graphene.

S3. The Effect of Al_2O_3 Removal on the Raman Spectra of Al_2O_3-coated 1LG

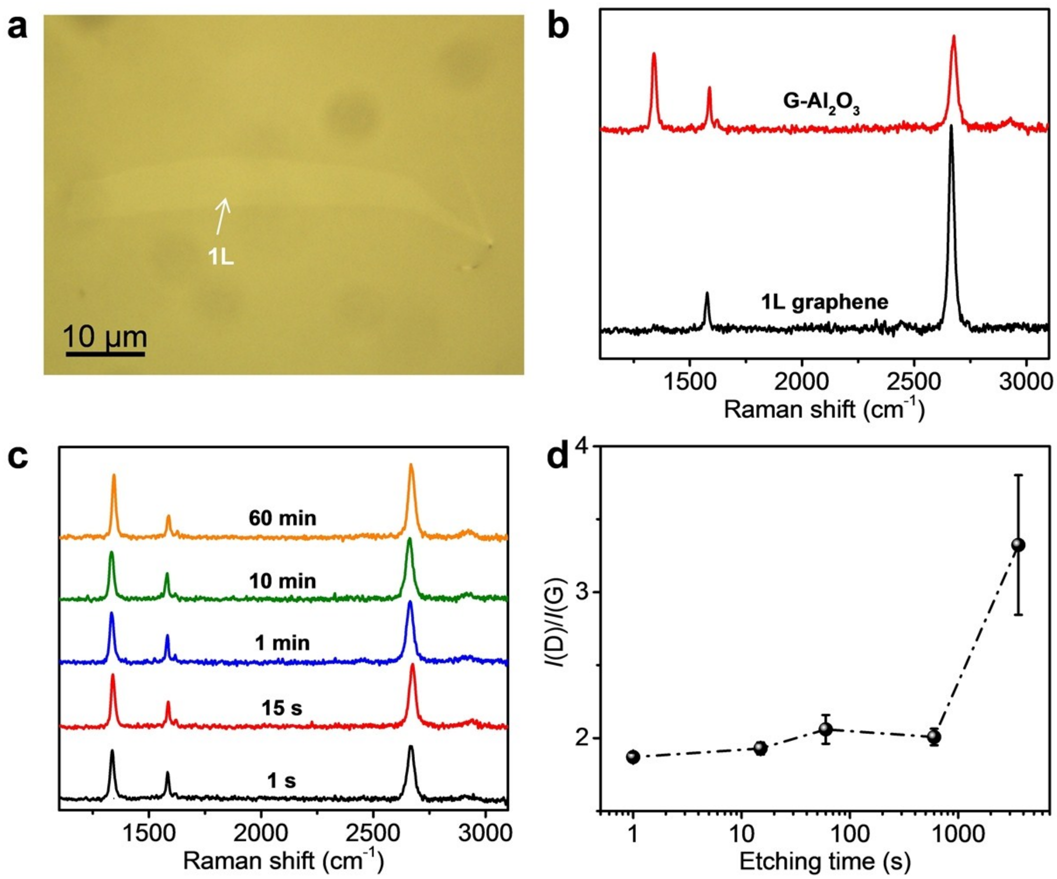

Fig. S3. (a) Optical image of an exfoilated monolayer graphene (1LG) transferred onto sapphire substrate. (b) Raman spectra of the 1LG before (black) and after (red) treated by Al_2O_3 plasmas with a power of 5 W for 15 min. (c) Raman spectra of Al_2O_3-coated 1LG as a function of wet etch time in hydrofluoric acid (HF) dilute solutionn (DI water: HF = 100:1). (d) The dependence of I_D/I_G ratio on the HF etch time.

S4. Raman Spectra of Graphene with Different Layer Thicknesses

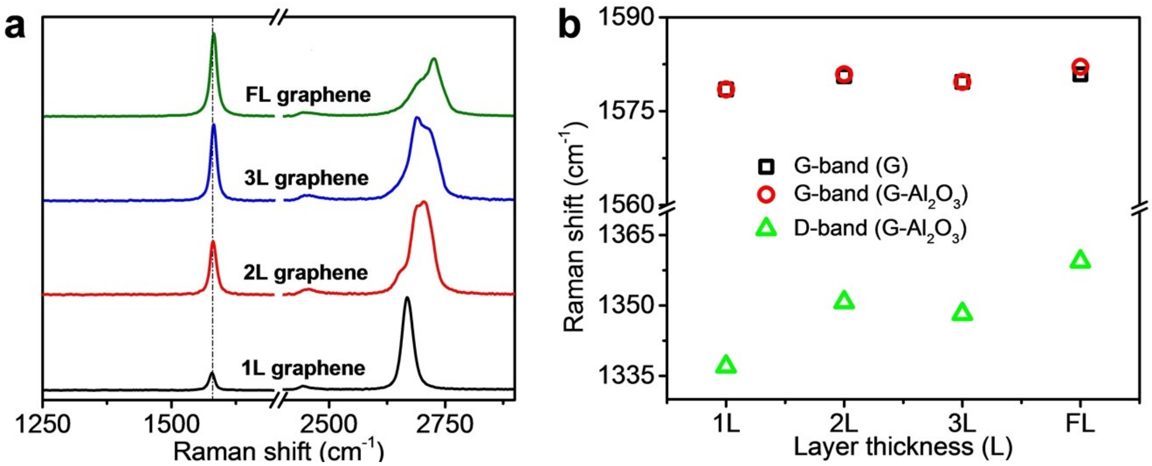

Fig. S4. (a) Raman spectra of as-prepared 1L to FL graphene on SiO_2/Si substrate shown in Fig. 1b. (b) The evolution of Raman shift for 1L to FL graphene subjected to Al_2O_3 plasma for a fixed time of 10 min.

S5. Controlled Creation and Removal of Defects in Graphene Monolayer and Few-Layers

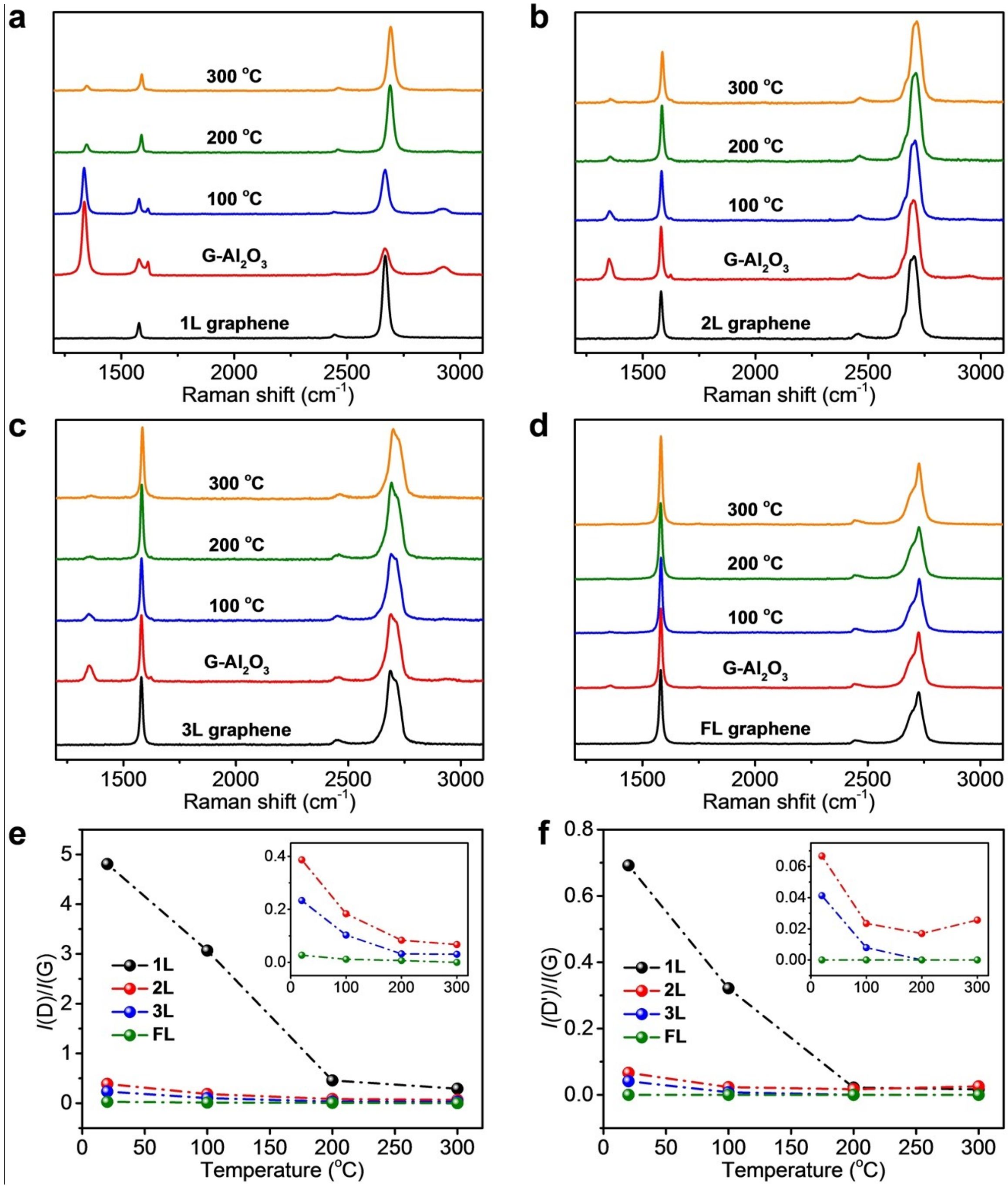

Fig. S5. Controlled creation and removal of defects in graphene monolayer and few-layers via moderate annealing. (a-d) Raman spectra of the defective graphene as a function of annealing temperature: (a) monolayer, (b) bilayer, (c) trilayer, and (d) few-layers. (e,f) The dependence of (e) I_D/I_G and (f) $I_{D'}/I_G$ ratio on the annealing temperature for the Al_2O_3-plasma-treated monolayer to few-layer graphene. Insert in (e,f) shows the maginified curves for 2L, 3L, and FL graphene.

S6. Raman Peak Position and Width as a Function of Annealing Temperature

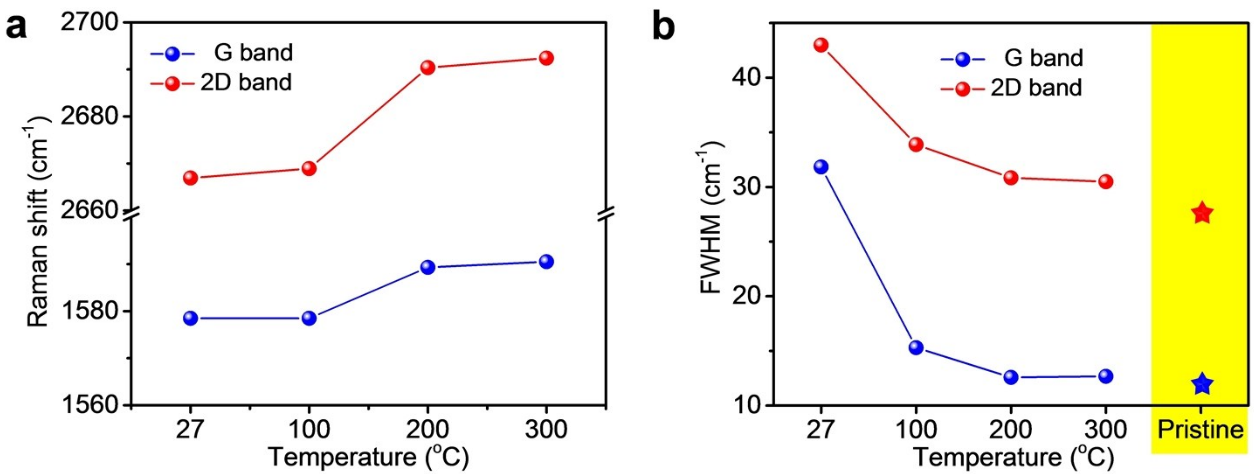

Fig. S6. (a) The frequency of G-band (blue) and 2D-band (red) as a function of annealing temperature for Al_2O_3-plasma-treated monolayer graphene (1LG). (b) The full width at half-maximum (FWHM) of G-band (blue) and 2D-band (red) as a function of annealing temperature. The above data was extracted from Raman spectra in Fig. 2a.

S7. Raman Mapping to Monitor the Reversible Defect Engineering in Graphene Few-Layers

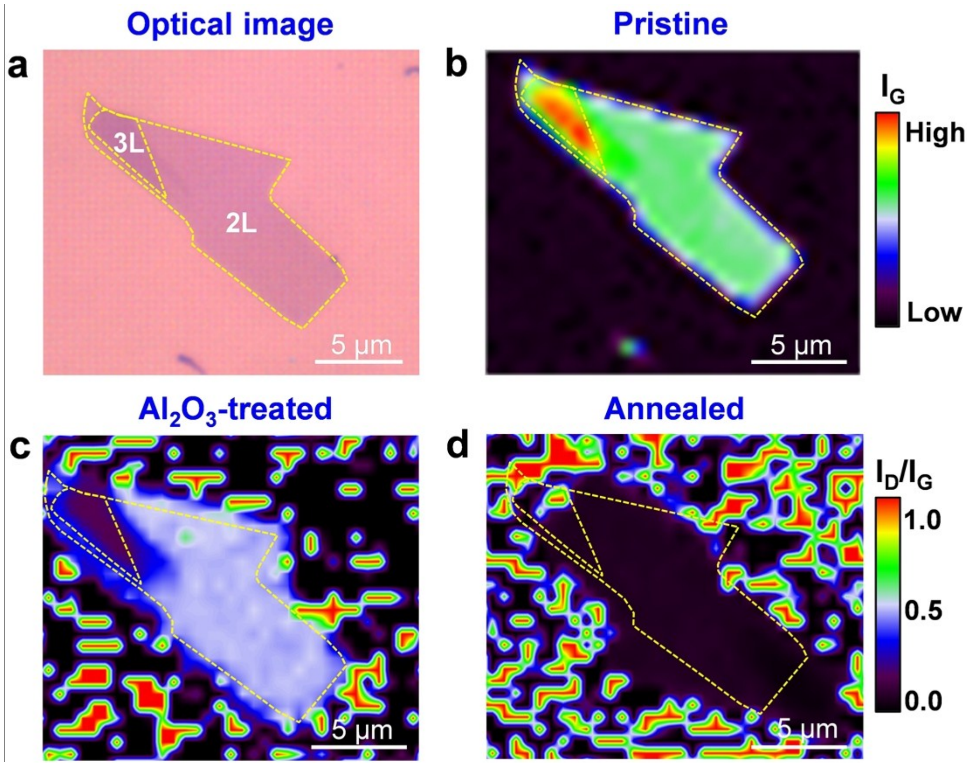

Fig. S7. Monitoring of the reversible defect engineering in graphene via Raman mapping. (a) Optical image and (b) G peak intensity mapping of the pristine 2L/3L graphene. (c,d) I_D/I_G intensity ratio mapping for the Al_2O_3-treated same sample (c) before and (d) after annealing at 300 ^oC.

S8. Raman Measurement of Al_2O_3-Plasma-Treated Monolayer MoS_2

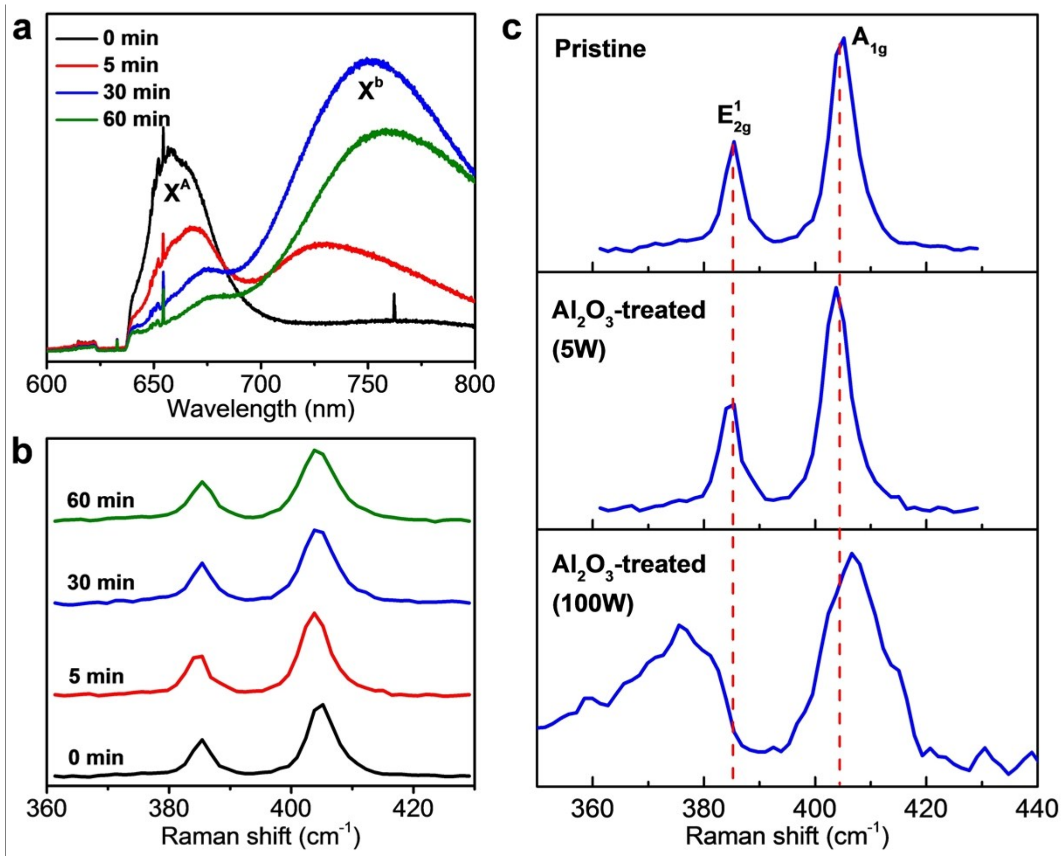

Fig. S8. Raman and photoluminescence (PL) characterization of defects in monolayer MoS_2 (1L-MoS_2). (a) PL and (b) Raman spectra of an exfoliated 1L-MoS_2 with increasing Al_2O_3 plasma treatment time. (c) Raman spectra for the pristine (top), low-power (middle), and high-power (bottom) Al_2O_3-plasma-treated 1L-MoS_2.

S9. AFM Characterization of Al_2O_3 Thin Layers on SiO_2/Si Substrates

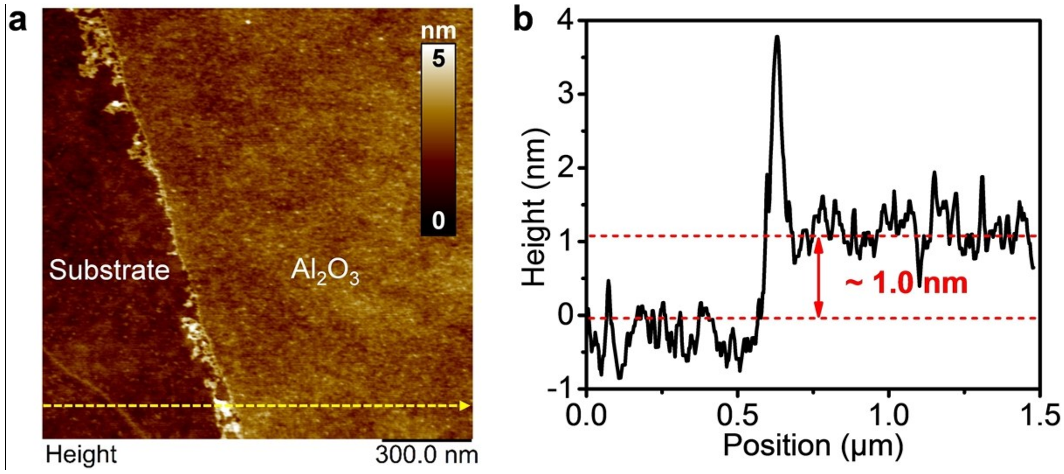

Fig. S9. (a) AFM image of a thin Al_2O_3 layer deposited on SiO_2/Si substrate with a power of 5 W for 5 min. (b) The cross-sectional profile along the yellow dotted line in (a).

S10. Morphological Characterization of Ultrathin Al_2O_3-Coated 2D Layers

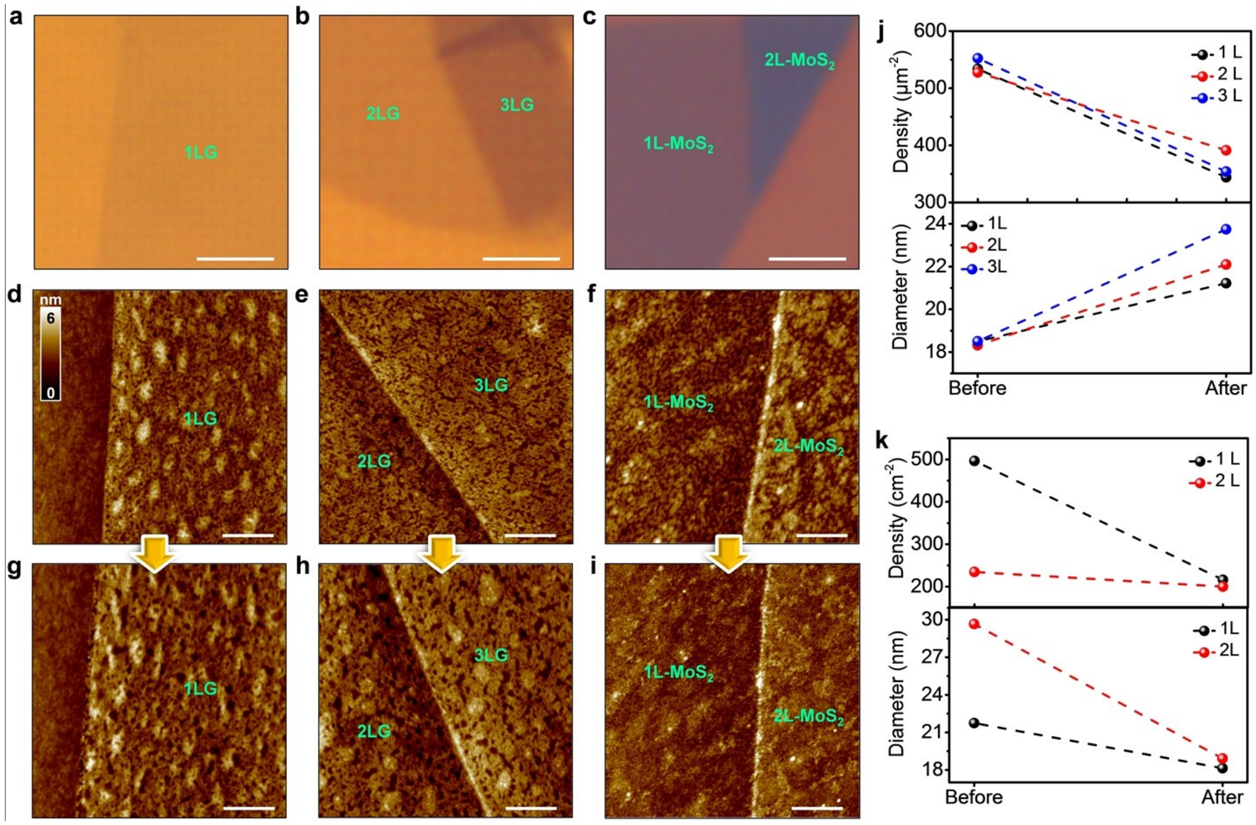

Fig. S10. *In situ* morphological characterization of ~ 1-nm-thick Al_2O_3-coated 2D materials with different layer thicknesses. (a-c) Optical images of as-prepared (a) 1LG, (b) 2L/3LG, and (c) 1L/2L-MoS_2 on SiO_2/Si substrates. Scale bars in (a-c): 500 nm. (d-f) AFM images of Al_2O_3-coated (d) 1LG, (e) 2L/3LG, and (f) 1L/2L-MoS_2. (g-i) AFM images of Al_2O_3-coated (g) 1LG, (h) 2L/3LG, and (i) 1L/2L-MoS_2 after annealing at 300 ^{o}C. Scale bars in (d-i): 200 nm. (j,k) The effect of thermal annealing on the vacancy density (top) and diameter (bottom) on (j) graphene and (k) MoS_2 surfaces.